Balanced Charge Carrier Transport Mediated by Quantum Dot Film Post-Organization for Light-Emitting Diodes Applications

Yuljae Cho,[a,*] Jongchul Lim,[b,h] Meng Li,[c,d] Sangyeon Pak,[e] Zhao-Kui Wang,[d] Ying-Guo Yang,[f] Antonio Abate,[c] Zhe Li,[g] Henry J. Snaith,[h] Bo Hou,[i,*] SeungNam Cha[e,*]

[a]University of Michigan – Shanghai Jiao Tong University Joint Institute, Shanghai Jiao Tong University, 800 Dong Chuan Road, Minghang District, Shanghai 200240, China
Email: yuljae.cho@sjtu.edu.cn

[b]Graduate School of Energy Science and Technology, Chungnam National University, 99 Daehak-ro, Yuseong-gu, Daejeon 34134, Korea.

[c]Helmholtz-Zentrum Berlin für Materialien und Energie, Kekuléstraße 5, 12489 Berlin, Germany

[d]Jiangsu Key Laboratory for Carbon-Based Functional Materials & Devices, Institute of Functional Nano & Soft Materials (FUNSOM), Soochow University, Suzhou 215123, P. R. China

[e]Department of Physics, Sungkyunkwan University, 2066, Seobu-ro, Jangan-gu, Suwon, Gyeonggi-do, 16419 Republic of Korea
Email: chasn@skku.edu

[f]Shanghai Synchrotron Radiation Facility (SSRF), Zhangjiang Lab, Shanghai Advanced Research Institute, Chinese Academy of Sciences, 239 Zhangheng Road, Shanghai 201204, P. R. China

[g]School of Engineering and Materials Science, Queen Mary University of London, Mile End Road, London E1 4NS, United Kingdom

[h]Department of Physics, Clarendon Laboratory, University of Oxford, Parks Road, Oxford OX1 3PU, United Kingdom

[i]School of Physics and Astronomy, Cardiff University, 5 The Parade, Newport Road, Cardiff, CF24 3AA, United Kingdom
Email: houb6@cardiff.ac.uk

Abstract

In light-emitting diodes (LEDs), balanced electron and hole transport is of particular importance to achieve high rates of radiative recombination. Most of quantum dot (QD)-based LEDs, however, employ infinitesimal core-shell QDs which inherently have different electron and hole mobilities. As QDs are the core building blocks for QD-LEDs, the inherent mobility difference in the core-shell QDs causes significantly unbalanced charge carrier transport, resulting in detrimental effects on performances of QD-LEDs.

Herein, we introduce a post chemical treatment to reconstruct the QD films through the solvent-mediated self-organization process. The treatment using various poly-alkyl alcohol groups enables QD ensembles to transform from disordered-solid dispersion into ordered-superlattice and effectively modulate electron and hole mobilities, which leads to the balanced charge carrier transport. In particular, ethanol-treated QD films exhibit enhanced charge carrier lifetime and reduced hysteresis due to the balanced charge carrier transport, which is attributed to the preferential-facet oriented QD post-organization. As a result, 63%, 78%, and 54% enhancement in external quantum efficiency (EQE) were observed in red, green, and blue QD-LEDs, respectively. These results are of fundamental importance to understand both solvent-mediated QD film reconstruction and the effect of balanced electron and hole transport in QD-LEDs.

Keywords: Quantum dots, Post chemical treatments, Crystal orientations, Charge carrier transport, Light-emitting diodes

Introduction

Quantum dots (QDs) have been brought to the forefront of new high-performance displays and smart light-emitting diodes (LEDs) due to their fascinating physicochemical properties, such as size-tunable emission wavelengths, high color purity, high quantum yield, and low fabrication cost.[1-6] Attributed to the unique optical properties and inorganic nature, QD-LEDs provide excellent photo-stability, quantum efficiency, and narrow emission bandwidth.[3] Therefore, extensive researches have been carried out for high performance QD-LEDs via (i) development of synthesis methods for QDs with high photoluminescence quantum yield (PLQY), (ii) engineering device architecture to align energy band levels of electron/hole transport layers (ETL/HTL), and (iii) balancing charge carrier transport to reduce charge accumulations in devices to enhance radiative recombination of electron-hole pairs.[7-17] The combination of various approaches, in turn, lead to recent achievements in QD-LEDs with high external quantum efficiency (EQE), over 20% of red and green QD-LEDs and 8 % of a blue QD-LED based on cadmium selenide and zinc sulphide core-shell (CdSe@ZnS) QDs.[7]

Due to the intrinsic asymmetrical population of electron and hole trap densities, however, CdSe@ZnS QDs, have shown large mobility deviation between charge carriers within core CdSe and shell ZnS, resulting in unbalanced charge carrier transport in Cd-based QD-LEDs.[13,14,18] In addition, the unbalanced charge carrier transport forms space charges in QD-LEDs, leading to non-radiative recombination. In spite of the importance of achieving charge balanced QD building blocks, less attention has been paid on balancing the charge transport in QD solids without modifying currently well-developed QD-LED structures, and its effect on the performance of QD-LED has not been reported so far. In this regard, it is urgently required to develop a fundamental and a viable concept on a new strategy of balancing the charge carrier transport at the level of the emissive QD layer via surface chemical engineering, which can directly facilitate efficient radiative recombination leading to high efficiency electroluminescence (EL).[2,7,18-21]

Herein, we report that protic solvents, a group of poly-alkyl alcohols, effectively balance the charge carrier transport crossing QD films associated with reconstruction of QD solid films. We found that a preferential crystal orientation of ensemble QD solids were effectively controlled by soaking them in different types of protic solvents. The QD solids exhibited the ordered superlattice when they were treated by ethanol and 1-butanol. On the contrary, the disordered QD solid dispersion was formed when they were treated by other types of poly-alkyl alcohols. The difference in QD solids eventually resulted in different electron and hole mobility, exciton lifetime as well as hysteresis behaviors. In particular, a QD film treated by ethanol exhibited the uniform crystalline orientation, which leads to a longer exciton lifetime and consequently efficient radiative recombination. We further investigated the electronic characteristics of QD films via systematic analysis of mobilities of electrons and holes as a function of the poly-alkyl length of alcohols. We demonstrated that QD film treated by ethanol exhibited the most balanced charge carrier transport, leading to a negligible hysteresis behavior. On the other hand, the QD film treated by 1-propanol or 1-butanol showed significant hysteresis behavior due to the imbalance of charge carrier transport. The results revealed the relationship between the post-treatment and crystal order reconstruction, resulting in the improvement in QD-LED performances. Our findings, in particular, provide a base platform to further enhance the performance of QD-LEDs, which is directly applicable to the well-established structure.

Result and Discussion

To understand the origin of solvent effect in charge carrier dynamics, we synthesized typical CdSe@ZnS QDs according to the previous works and fabricated LEDs via a layer-by-layer fabrication method.[22-24] As-prepared CdSe@ZnS QDs were purified several times before dispersing into hexane at a concentration of 12.5 mgmL^{-1}. Figure 1(a) illustrates a QD solution in hexane under ambient and ultra-violet (UV 365 nm) light, respectively. The absolute solution-state PLQY was determined to be 80 ± 5 %. The transmission electron microscopy

(TEM) analysis revealed the characteristic cubic feature of as-prepared QDs.[22,24] As shown in Figure 1(b), (111) lattice fringes are observed, which is in good agreement with the results reported previously.[22,24] The bottom image of Figure 1(b) shows the histogram of QD sizes, revealing that the average size of QDs is 4.83 nm ± 1 nm and they have narrow size distribution with a standard deviation below 20%. Figure 1(c) shows absorption and PL spectra of a QD film without any ligand treatment. A negligible stoke shift is observed from the absorption and PL spectrum, indicating that CdSe core is well passivated by ZnS shell.

Generally, QDs are capped with organic ligands consisting of long-chain aliphatic ligands (8-18 carbons) to ensure their colloidal stability and solution processability. Therefore, a QD film directly deposited from the solution requires a ligand exchange and washing process in order to facilitate charge carrier transport in both lateral and vertical directions.[25-27] In order to understand the mechanism of surface ligand replacement, the solvent treatment using different kinds of poly-alkyl alcohol was performed on a QD film, and followed by Fourier-transform infrared spectroscopy (FTIR) measurement. As shown in Figure 1(d), these alcohol solvents exhibit significant effects on removing the long carbon chain ligands from the surface of the QD film, evidenced from a significant decrease in the vibration peaks of the $-CH_{as}$ (~2925 cm^{-1}) and $-CH_s$ (~ 2850 cm^{-1}).[28] After looking further into the FTIR measurement, different types of solution exhibit different degrees of ligand removal rates. It is found that ethanol is the most effective solvent in removing long chain ligands, even beyond methanol which is known to have the superior ability to remove ligands from the QD surface.[29] In addition, the ligand removal was independent of QD losing by comparing absorption (Figure S1 in Supporting Inforation (SI)) with FTIR spectra, which indicates that there is almost similar amount of QDs before and after the solvent treatment.

Following the studies on properties of solution phase QDs, we investigated the effect of the post-chemical treatment on the crystalline orientation of QD solid films. Basically, the post

treatment using polar protic solvents reconstructs QD orientations as QDs attached together to reduce the surface energy of the un-passivated surface after removal of ligand.[30,31] In particular, during the protonation reaction (generating protonated oleic acid and dissociation of zinc oleate), we found that ethanol treatment provides the best balance between ligand removal and QD colloidal stability which results in the formation of the preferred lattice orientations.[32,33] The real-time 2D grazing incidence X-ray diffraction (GIXRD) was performed through a high brightness synchrotron X-ray source. A strong scattering background from the diffraction patterns and the uniform diffraction rings appeared in QD films treated by poly-alkyl alcohol solvents are shown in Figure 2(a)-(f) together with the control film, i.e. no solvent treatment. It can be seen that QD films treated with ethanol (Figure 2(c)) and 1-butanol (Figure 2(e)) exhibit a uniform diffraction ring, indicating that the film has the uniform crystalline orientation. The uniform crystalline orientation is known to assist efficient recombination of electrons and holes in the film, facilitating optimum EL performance of a QD-LED.[34-36]

In addition, the GIXRD reveals that the crystal (k01) diffractions become preferentially oriented normal to the substrate when QD films were treated by ethanol and 1-butanol, while the untreated films exhibited powder-like diffuse rings in the diffraction pattern indicating a random crystallite orientation.[34-36] The 2D GIXRD pattern of the ethanol sample has a more pronounced ring-like and less textured appearance than the other samples. The (101), (103) and (203) peaks can be indexed from azimuthally integrated scattering intensity of different GIXRD profiles along the ring. The GIXRD results provide clear evidence of preferred lattice orientation in reconstructed QD films assisted by different protic solvents.[34] Because the internal structure and crystal properties of QD films mainly determines the dynamic charge transport characteristics and the EL performance, the GIXRD results suggest that a QD-LED treated by ethanol would have an optimum device performance.

The effect of chemical treatment on exciton dynamics in QD solids is investigated via time-resolved photoluminescence (TRPL). Figure 3(a) shows a PL spectrum of a QD film treated by ethanol as a representative, which shows a peak at 573 nm. Notably, other QD films treated by other poly-alkyl alcohol solvents also exhibited a peak at the same wavelength (Figure S2(a) in SI). This result together with the absorption spectra in Figure S1 indicates that there were no bandgap variations induced by different protic solvents. By employing a pulse laser with wavelength at 573 nm, TRPL measurement was conducted on each QD film (Figure S2(b)-(f) in SI). The charge carrier lifetime was then extracted by fitting TRPL decay curves with a biexponential decay function where the first exponent (τ_1) is related to a high rate of transition of interparticle charge and energy transfer, and the second exponent (τ_2) is attributed to charge carrier recombination.[37-40] Figure 3(b) illustrates the exciton lifetime of each QD film treated by different types of poly-alkyl alcohol solvents, and fitted results are summarized in Table S1 in SI. The long charge carrier lifetime (τ_2) observed in ethanol and 1-butanol treated QD films and enhanced PL intensity from both films (Figure S3 in SI) indicate that less surface defects exist in the QD films, which is attributed to the uniform crystalline orientation within the QD films.[41-43]

Measurement of electron and hole mobility of QD films treated by different poly-alkyl alcohol solvents was carried out by extracting space-charge-limited current (SCLC) as shown in Figure S4 and S5 in SI. It is worth noting that the same hole injection layer (HIL) (poly(3,4-ethylenedioxythiophene)-poly(styrenesulfonate), or PEDOT:PSS), HTL (poly(9,9-dioctylfluorene-alt-N-(4-sec-butylphenyl)-diphenylamine, or TFB), and ETL (zinc oxide nanoparticles, or ZnO NPs) were used for electron only and hole only devices in order to attain consistent results with QD-LEDs. To completely remove residual solvent, we performed a thermal annealing at each step of the layer deposition, which prevented the solvent erosion effect. In particular, solvents, hexane and chlorobenzene, were chosen for the QD and TFB layer because they are complete orthogonal solvents and therefore each solvent hardly erodes

the other layer.[44] The structures of electron only and hole only devices were ITO/ ZnO NPs/ CdSe@ZnS QDs/ ZnO NPs/ Al, and ITO/ PEDOT:PSS/ TFB/ CdSe@ZnS QDs/ TFB/ Au, respectively. Then, the ratio of the difference in electron and hole mobility is calculated as shown in Figure 3(c) and Table S2 in SI.[3] Electron and hole mobility mismatch is extremely high (~ 25 %) in a QD film treated by 1-propanol, which is in good agreement with severe hysteresis of the QD-LED treated by 1-propanol as shown in Figure 3(d). In addition, the QD films treated by 1-propanol show high hysteresis over various scanning ranges, as shown in Figure S6(a)-(c) in SI. On the contrary, QD films treated by methanol and ethanol exhibited a relatively low mobility mismatch, and therefore QD-LEDs treated by methanol and ethanol showed negligible hysteresis as shown in Figure 3(d) and Figure S6(a)-(c) in SI. In addition, charge balance in the QD-LED treated by ethanol was again confirmed by electron and hole currents from the SCLC devices as shown in Figure S4 and S5 in SI whereas other QD-LEDs show that one to two orders difference in electron and hole currents, indicating imbalance of electron and hole mobility and therefore charge carrier transport.[2] Despite of negligible hysteresis in a QD film treated by methanol, a hysteresis curve exhibited a higher current level due to leakage current, which resulted in poor device performance (Figure 4). The leakage current in the QD-LED treated by methanol is due to the formation of the extra trap states as the methanol treatment was demonstrated to be offensive to QDs surface.[45-47] With the 1-butanol and 1-hexanol treatments, the mismatches between electron and hole mobilities within the films are slightly higher than that of the QD films treated by ethanol, and therefore both devices exhibit visible hysteresis behaviors as shown in Figure 3(d) and Figure S6 in SI. The different electronic properties of each QD film are closely related to the film crystallinity changes in accordance with the applied poly-alkyl alcohol solvents, which is in good agreement with previous reports on the effects of crystallinity on the performance of electronic devices.[18,48] As revealed by both the SCLC measurements and the hysteresis curves of QD films, charge carrier transport is facilitated and also optimally balanced in the QD-LEDs treated by the

ethanol. It is worth noting that we kept all other conditions in SCLC devices the same such as thickness of each layer and processes, except for the solvent treatments to QD films. Because the travel distances for electrons and holes were fixed for all SCLC devices, differences in charge carrier transport in SCLC devices are due to the differences in electron and hole mobility of QD films treated by different solvent, suggesting the balanced charge transport from the QD film level. Electrical and photo-electrical characteristics are summarized in Table S3 in SI. We find the performance of QD-LEDs follows the trend of the summarized results, and insightful discussions will be provided in the following sections.

Figure 4(a) shows a flat-band energy level diagram of a QD-LED with a structure of ITO/ PEDOT:PSS/ TFB/ QDs/ ZnO/ Al. The energy level of each layer was referred to literature reported previously.[2,3] This structure in our study was used on purpose because it is the most frequently employed structure with the highest EQE reported for CdSe@ZnS QD-LEDs.[49] Therefore, our work will give a general guideline to the research community for an effect of different poly-alkyl alcohol solvents for QD film treatment, and directly contribute to future researches without modifying any device structures.[2,3,9,50]

Current density (J) and luminance (L) characteristics as a function of applied bias are shown in Figure 4(b) and (c). The QD-LEDs treated by ethanol (red), 1-propanol (blue), and 1-butanol (green) show low leakage currents at low bias, i.e., below turn-on voltage. As the applied voltage increases, the QD-LED treated by ethanol (red) shows much higher luminance, which is attributed to the formation of the uniform crystal orientation in QD films (Figure 2) and consequently balanced electron and hole transport (Figure 3(c)). On the contrary, the QD-LEDs treated by 1-propanol (blue), 1-butanol (green), and 1-hexanol (purple) exhibited limited current density and low luminance at high voltage, indicating that radiative recombination under a high electric field became less efficient than that of a QD-LED treated by ethanol due to unbalanced charge carrier transport. In particular, the QD-LED treated by 1-propanol showed

a fast drop of EQE (Figure 4(d)), which resulted from severely unbalanced charge carrier transport because the space charges formed in the device caused rapid deterioration of the device under the operational condition.[4] In spite of high luminance of the QD-LED treated by methanol (black), high leakage current at the low bias condition led to poor device performance (Table 1), which is due to the formation of the non-uniform film and consequently charge traps formed (Figure 2). This is in good agreement with results from SCLC and QD-LED measurements in Figure 3(d) and Figure 4(b).

The QD-LED treated by ethanol outperforms in comparison to other QD-LEDs, as shown in Figure 4(d). For example, EQE (η_{EQE}) and current efficiency (η_A) of the QD-LED treated by ethanol at 1000 cdm^{-2} luminance exhibits 2.9 and 13.2 times higher than that of the QD-LED treated by 1-hexanol. The results of QD-LEDs performance are well consistent with all characterization results discussed in Figure 2 (GIXRD) and Figure 3 (TRPL and SCLC), indicating that a judicious selection of poly-alkyl alcohol solvent to treat a QD film is of particular importance for the device performance. Table 1 summarizes the detailed performance parameters of QD-LEDs treated by the different solvents. In addition, a grey line in Figure 4(b)-(d) shows a QD-LED without any solvent treatment to demonstrate the effect of the QD treatment on optoelectronic properties of a QD film. Because of insulating ligands on the surface of a QD film, i.e. high series resistance, the device turns on at higher voltage (3.6 V) and exhibited lower maximum luminance (L_{max} 16660 cdm^{-2}). As shown in Figure S7 in SI, electroluminescence (EL) spectrum of the QD-LED treated by ethanol illustrates a symmetric emission peak at 555 nm with a narrow full-width at half-maximum (FWHM) of 25.39 and 25.74 nm at EQE_{max} and L_{max}, respectively. EL spectrum of QD-LEDs treated by other solvents are also shown in Figure S7 and FWHM at EQE_{max} and L_{max} are summarized in Table S4 in SI. It is worth noting that ZnO layers on QD films without and with solvent treatment exhibited similar surface roughness and morphology (Figure S8 in SI), indicating that the difference in

device performances is due to crystalline orientation, charge carrier mobilities, and hysteresis, not due to the quality of the ZnO layers on QD films treated by the different solvents.

We further expanded the post-treatment approach to attain high performance QD-LEDs by finely tuning thickness of QD and functional layers where PLQY of red, green, and blue QDs was approximately 80 ± 5 % for all colors. To ensure that QD films before and after the ethanol treatment do not form cracks, we performed AFM measurement. As shown in Figure S9 in SI, the QD film treated by ethanol did not show any observable cracks. As shown in Figure 5(a)-(c), high EQE values were achieved in red, green, and blue QD-LEDs, which showed approximately 63%, 78%, and 54% enhancement compared to the QD-LEDs without any solvent treatment where the maximum EQE was 13.55, 7.17, and 3.73%, for red, green, and blue QD-LEDs, respectively. Further details of the QD-LEDs performance are shown in Table 2 and Figure S10-S15 in SI. All QD-LEDs exhibited stable performance without drooping until at 1000 cd/m^2, a level of which used for display technology. QD-LEDs maintained over 90% of their original performances, which were 13.55 to 13.54%, 7.17 to 7.03%, and 3.73 to 3.43% for red, green, and blue QD-LEDs, respectively.[51] Figure S16 shows Commission International de l'Eclairage (CIE) chromaticity diagram of the QD-LEDs at L_{max}. Corresponding coordinates are close to the spectral locus, (X,Y) = (0.6761, 0.3229), (0.3787, 0.6137), and (0.1301, 0.0665) for red, green and blue QD-LEDs, respectively, indicating that the QD-LEDs exhibit very saturated and pure monochromatic colors, which is ideal for future display applications.[2,3,52] Average EQE values shown in Figure 5(d) were extracted from each 15 individual devices of red, green, and blue QD-LEDs as shown in Table 2, which demonstrated stable QD-LEDs performance in all colors.

The effect of poly-alkyl alcohol solvents on QD films was thoroughly investigated in this work. First, crystal orientations in QD films varied with respect to the poly-alkyl alcohol solvents

applied to the QD films. The QD films treated by ethanol and 1-butanol exhibited a uniform diffraction ring, meaning the uniform crystalline orientation over the QD films. The uniform crystalline orientation facilitated efficient recombination of electrons and holes in the QD films, contributing to the optimum EL performance of a QD-LED. Second, TRPL measurement further revealed that QD films treated by ethanol and 1-butanol had a longer charge carrier lifetime, which was attributed to the uniform crystalline orientation on the QD films. Third, comparing the QD films treated by ethanol and 1-butanol, we found that the QD film treated by ethanol demonstrated particularly well-balanced charge carrier transport due to almost identical electron and hole mobility, which resulted in the negligible hysteresis effect in the QD-LEDs. As a result, QD-LEDs treated by ethanol outperformed QD-LEDs without treatments and treated by other types of poly-alkyl alcohol solvents, achieving high luminance and EQE values in green QD-LEDs. To further add a generality of our new approach, we applied this method to QDs with different emission wavelengths, namely, red (~630 nm) and blue (~465 nm). The solvent treatment revealed that this new approach had the same effect to all RGB QDs, exhibiting significant enhancement in device performance, in particular, over 12% average EQE in red QLEDs with the peak luminance 53610 cdm^{-2}. In addition, we observed low efficiency roll-off in blue QLEDs. This is attributed to the well-balanced charge carrier transport in ethanol treated blue QLEDs and also high bandgap of blue QDs which made the QLEDs less susceptible to the high current.[53,54] Overall, all of RGB QD-LEDs exhibited negligible efficiency roll-off until 1000 cdm^{-2} luminance, indicating that our new method can provide an effective way to fabricate high and stable device performance. Our findings provide valuable information on the correlated relationships among the post-treatment, the crystalline orientation, the charge carrier lifetime, and balanced charge carrier transport. In addition, this result is directly applicable to the well-established QD-LED structures without modifying the structures for balancing charge carrier transport.

Conclusion

We introduced a post chemical treatment to a QD film for turning intrinsic charge unbalanced CdSe@ZnS core-shell QDs into a charge balanced QD film. QD solids were built with a preferential crystal orientation by treating poly-alkyl alcohol solvents. The QD film treated by ethanol formed the uniform crystalline orientation, which led to a longer exciton lifetime. In addition to the uniform film, the QD film treated by ethanol exhibited the optimum charge balance of the QD film, indicating that the post-chemical treatment effectively modified charge unbalanced individual core-shell QD to attain charge balanced QD solid matrix. The charge balanced QD solids through the ethanol treatment were used as building blocks for a QD-LED. The device demonstrated significantly enhanced electrical and opto-electrical properties compared to QD-LEDs treated by other types of poly-alkyl alcohol solvents, which was found to be originated from a longer exciton lifetime and balanced charge transport associated to the formation of uniform crystalline orientation. Using the post-treatment strategy, red, green, and blue QD-LEDs exhibited 63%, 78%, and 54% of EQE improvement where maximum EQE was 13.55, 7.17, and 3.73%, for red, green, and blue QD-LEDs, respectively. The result highlights the significance of developing a new charge balance strategy at the level of the emissive QD layer mediated by judicious selection of the poly-alkyl alcohol solvent.

Experimental

Material preparation: Pixelated ITO substrates, PEDOT:PSS solution and TFB powder were purchased from Ossila. ITO substrates and PEDOT:PSS were used as received and TFB was dissolved in chlorobenzene at the concentration of 8 $mgmL^{-1}$. CdSe@ZnS QDs were synthesized according to the previous works, and the concentration of the QDs was 12.5 $mgmL^{-1}$ in Hexane.[22-24] ZnO nanoparticles (NPs) were synthesized using previously reported recipe by our group.[55,56]

GIXRD measurement: The grazing incidence X-ray diffraction (GIXRD) measurements were performed at the BL14B1 beamline of the Shanghai Synchrotron Radiation Facility (SSRF) using X-ray with a wavelength of 1.24 Å. Two-dimensional (2D) GIXRD patterns were acquired by a MarCCD mounted vertically at a distance ~223 mm from the sample with a grazing incidence angle of 0.1°and 0.3°, and an exposure time of 20 sec. The 2D GIXRD patterns were analyzed using the FIT2D software and displayed in scattering vector q coordinates. The in-situ tensile XRD experimental was measured by the transmission mode, and the flexible PSCs were pasted on the lateral side of the sample holder and placed at the vertical of X-ray incidence direction.

Device fabrication: Pixelated ITO substrates were cleaned using acetone, 1-propanol, and deionized water for 10 minutes, respectively, and then Ozone treatment was carried out on the substrates for 5 minutes. PEDOT:PSS was spin-coated at the speed of 4000 rpm for 60 seconds and then baked at 150 ℃ for 30 minutes. After the annealing, the PEDOT:PSS coated substrates were transferred to a nitrogen-filled glove box. TFB was spin-coated on the PEDOT:PSS layer at the speed of 4000 rpm for 45 seconds, which was followed by thermal annealing at 130 ℃ for 30 minutes. CdSe@ZnS QDs were spin-coated on the TFB layer at a speed of 4000 rpm for 30 seconds, and the protic solvent was loaded on to the QD layer for surface treatment for 60 seconds. Using the same solvent, the washing process was performed for two times. Finally, ZnO NPs were spin-coated on the QD layer at the speed of 3000 rpm for 30 seconds. The QD

and ZnO layers were thermally annealed at 90 ℃ for 10 minutes, and then Aluminum (100 nm thick) was deposited on the ZnO layer using a thermal evaporator. The active area was 0.045 cm^2. The optimized thickness for QD-LEDs is ~46 nm for PEDOT:PSS and TFB, ~ 20 nm for QDs, and ~ 50 nm for ZnO nanoparticles.

Device characterization: QD-LEDs were passivated prior to measurements and were measured using HAMAMATSU PMA-12 connected with Keithley 2400 source meter at room temperature under ambient air condition. For space charge limited current (SCLC) measurements, electron only and hole only devices were fabricated with a structure of (1) ITO/ ZnO/ QD/ ZnO/ Al and (2) ITO/ PEDOT:PSS/ TFB/ QD/ TFB/ Au, respectively. I-V curves were measured using Keithley 4200, and then the I-V curves were fitted using the Mott-Gurney law to extract electron and hole mobility where relative permittivity of CdSe@ZnS QDs was assumed to be 9.5.[37,57] Hysteresis measurements were performed using the QD-LEDs treated by each protic solvent with various scanning range, (i) -0.5 ~ 3 V, (ii) -1 ~ 5 V, and (iii) -2 ~ 8 V. Each step and scanning speed were fixed for all measurements. The cross-sectional TEM images of the QD-LEDs were characterized via high-resolution (HR)-STEM (FEI Tecnai F20 FEGTEM), and the samples were sliced using a focused ion beam (FIB) system (Dual-Beam FIB, FEI Helios Nanolab SEM/FIB).

Supporting Information

Absorption spectra of QD films, PL and time-resolved PL curves of QD films, extracted parameters by fitting time-resolved PL curves, SCLC curves, electron and hole mobility, hysteresis curves, EL of QD-LEDs, FWHM characteristics, 3D AFM images of ZnO and QD films morphology, Red, Green, and Blue QD-LED device characteristics, CIE coordinates of Red, Green, and Blue QD-LEDs.

Conflicts of interest

There are no conflicts to declare.

State of contributions

Y.C., B.H., and S.C. planned the project and wrote the manuscript. J.L. and H.J.S. performed TRPL measurements and analysis. S.P. performed AFM measurement and analysis. M.L., Z.-K.W., Y.-G.Y., and A.A., and Z.L. investigated GIXRD measurements and contributed to the interpretation of the data.

Acknowledgements

Y.C. and J.L. contributed equally to this work. Y.C. would like to thank UM-SJTU JI, Shanghai Jiao Tong University, for research support. This work was supported by research fund of Chungnam Nation University. B.H. acknowledges the financial support by the Cardiff University. This was supported by the National Research Foundation (NRF) of Korea (2019R1A2C1005930).

References

1. Murray, C.; Kagan, C.; Bawendi, M. Self-Organization of CdSe Nanocrystallites into Three-Dimensional Quantum Dot Superlattices. *Science* **1995**, 270, 1335-1338.

2. Dai, X.; Zhang, Z.; Jin, Y.; Niu, Y.; Cao, H.; Liang, X.; Chen, L.; Wang, J.; Peng, X. Solution-Processed, High-Performance Light-Emitting Diodes Based on Quantum Dots. *Nature* **2014***,* 515, 96-99.

3. Yang, Y.; Zheng, Y.; Cao, W.; Titov, A.; Hyvonen, J.; Manders, J. R.; Xue, J.; Holloway, P. H.; Qian, L. High-Efficiency Light-Emitting Devices Based on Quantum Dots with Tailored Nanostructures. *Nat. Photon.* **2015***,* 9, 259-266.

4. Sun, Q.; Wang, Y. A.; Li, L. S.; Wang, D.; Zhu, T.; Xu, J.; Yang, C.; Li, Y. Bright, Multicoloured Light-Emitting Diodes Based on Quantum Dots. *Nat. Photon.* **2007**, 1, 717-722.

5. Choi, M. K.; Yang, J.; Kim, D. C.; Dai, Z.; Kim, J.; Seung, H.; Kale, V. S.; Sung, S. J.; Park, C. R.; Lu, N. Extremely Vivid, Highly Transparent, and Ultrathin Quantum Dot Light-Emitting Diodes. *Adv. Mater.* **2018**, 30, 1703279.

6. Li, X.; Zhao, Y.; Fan, F.; Levina, L.; Liu, M.; Quintero-Bermudez, R.; Gong, X.; Quan, L. N.; Fan, J.; Yang, Z.; Hoogland, S.; Voznyy, O.; Lu, Z.; Sargent, E. H. Bright Colloidal Quantum Dot Light-Emitting Diodes Enabled by Efficient Chlorination. *Nat. Photon.* **2018**, 12, 159-164.

7. Shen, H.; Gao, Q.; Zhang, Y.; Lin, Y.; Lin, Q.; Li, Z.; Chen, L.; Zeng, Z.; Li, X.; Jia, Y. Visible Quantum Dot Light-Emitting Diodes with Simultaneous High Brightness and Efficiency. *Nat. Photon.* **2019**, 13, 192-197.

8. Liu, Y.; Jiang, C.; Song, C.; Wang, J.; Mu, L.; He, Z.; Zhong, Z.; Cun, Y.; Mai, C.; Wang, J. Highly Efficient All-Solution Processed Inverted Quantum Dots Based Light Emitting Diodes. *ACS Nano* **2018**, 12, 1564-1570.

9. Ban, M.; Zou, Y.; Rivett, J. P.; Yang, Y.; Thomas, T. H.; Tan, Y.; Song, T.; Gao, X.; Credington, D.; Deschler, F. Solution-Processed Perovskite Light Emitting Diodes with Efficiency Exceeding 15% through Additive-Controlled Nanostructure Tailoring. *Nat. Commun.* **2018**, 9, 3892.

10. Zhang, Z.; Ye, Y.; Pu, C.; Deng, Y.; Dai, X.; Chen, X.; Chen, D.; Zheng, X.; Gao, Y.; Fang, W. High-Performance, Solution-Processed, and Insulating-Layer-Free Light-Emitting Diodes Based on Colloidal Quantum Dots. *Adv. Mater.* **2018**, 30, 1801387.

11. Zhang, H.; Chen, S.; Sun, X. W. Efficient Red/Green/Blue Tandem Quantum-Dot Light-Emitting Diodes with External Quantum Efficiency Exceeding 21%. *ACS Nano* **2017**, 12, 697-704.

12. Lee, B. R.; Yu, J. C.; Park, J. H.; Lee, S.; Mai, C.; Zhao, B.; Wong, M. S.; Jung, E. D.; Nam, Y. S.; Park, S. Y. Conjugated Polyelectrolytes as Efficient Hole Transport Layers in Perovskite Light-Emitting Diodes. *ACS Nano* **2018**, 12, 5826-5833.

13. Zhang, X.; Lin, H.; Huang, H.; Reckmeier, C.; Zhang, Y.; Choy, W. C.; Rogach, A. L. Enhancing the Brightness of Cesium Lead Halide Perovskite Nanocrystal Based Green Light-Emitting Devices through the Interface Engineering with Perfluorinated Ionomer. *Nano Lett.* **2016**, 16, 1415-1420.

14. Lee, K.; Han, C.; Jang, E.; Jo, J.; Hong, S.; Hwang, J. Y.; Choi, E.; Hwang, J.; Yang, H. Full-Color Capable Light-Emitting Diodes Based on Solution-Processed Quantum Dot Layer Stacking. *Nanoscale* **2018**, 10, 6300-6305.

15. Diroll, B. T.; Schaller, R. D. Shape-Selective Optical Transformations of CdSe Nanoplatelets Driven by Halide Ion Ligand Exchange. *Chem. Mater.* **2019**, 31, 3556-3563.

16. Smith, A. M.; Nie, S. Semiconductor Nanocrystals: Structure, Properties, and Band Gap Engineering. *Acc. Chem. Res.* **2009**, 43, 190-200.

17. Lim, S. J.; Schleife, A.; Smith, A. M. Optical Determination of Crystal Phase in Semiconductor Nanocrystals. *Nat. Commun.* **2017**, 8, 14849.

18. Gao, Y.; Peng, X. Photogenerated Excitons in Plain Core CdSe Nanocrystals with Unity Radiative Decay in Single Channel: The Effects of Surface and Ligands. *J. Am. Chem. Soc.* **2015**, 137, 4230-4325.

19. Yang, Y.; Qin, H.; Jiang, M.; Lin, L.; Fu, T.; Dai, X.; Zhang, Z.; Niu, Y.; Cao, H.; Jin, Y. Entropic Ligands for Nanocrystals: From Unexpected Solution Properties to Outstanding Processability. *Nano Lett.* **2016**, 16, 2133-2138.

20. Shen, H.; Cao, W.; Shewmon, N. T.; Yang, C.; Li, L. S.; Xue, J. High-Efficiency, Low Turn-on Voltage Blue-Violet Quantum-Dot-Based Light-Emitting Diodes. *Nano Lett.* **2015**, 15, 1211-1216.

21. Zheng, T.; Choy, W. C.; Ho, C.; Wong, W. Improving Efficiency Roll-Off in Organic Light Emitting Devices with a Fluorescence-Interlayer-Phosphorescence Emission Architecture. *Appl. Phys. Lett.* **2009**, 95, 133304.

22. Hou, B.; Parker, D.; Kissling, G. P.; Jones, J. A.; Cherns, D.; Fermín, D. J. Structure and Band Edge Energy of Highly Luminescent $CdSe_{1-x}Te_x$ Alloyed Quantum Dots. *J. Phys. Chem. C* **2013**, 117, 6814-6820.

23. Benito-Alifonso, D.; Tremel, S.; Hou, B.; Lockyear, H.; Mantell, J.; Fermin, D. J.; Verkade, P.; Berry, M.; Galan, M. C. Lactose as a "Trojan Horse" for Quantum Dot Cell Transport. *Angew. Chem. Int. Ed.* **2014**, 53, 810-814.

24. Hou, B.; Benito-Alifonso, D.; Webster, R.; Cherns, D.; Galan, M. C.; Fermín, D. J. Rapid Phosphine-Free Synthesis of CdSe Quantum Dots: Promoting the Generation of Se Precursors Using a Radical Initiator. *J. Mater. Chem. A* **2014**, 2, 6879-6886.

25. Tang, J.; Kemp, K. W.; Hoogland, S.; Jeong, K. S.; Liu, H.; Levina, L.; Furukawa, M.; Wang, X.; Debnath, R.; Cha, D.; Chou, K. W.; Fischer, A.; Amassian, A.; Asbury, J. B.; Sargent, E. H. Colloidal-Quantum-Dot Photovoltaics Using Atomic-Ligand Passivation. *Nat. Mater.* **2011**, 10, 765-771.

26. Jo, J. W.; Kim, Y.; Choi, J.; Pelayo García de Arquer, F.; Walters, G.; Sun, B.; Ouellette, O.; Kim, J.; Proppe, A. H.; Quintero-Bermudez, R.; Fan, J.; Xu, J.; Tan, C. S.; Voznyy, O.; Sargent, E. H. Enhanced Open-Circuit Voltage in Colloidal Quantum Dot Photovoltaics via Reactivity-Controlled Solution-Phase Ligand Exchange. *Adv. Mater.* **2017**, 29, 1703627.

27. Jo, J. W.; Choi, J.; Pelayo García de Arquer, F.; Seifitokaldani, A.; Sun, B.; Kim, Y.; Ahn, H.; Fan, J.; Quintero-Bermudez, R.; Kim, J.; Choi, M.; Baek, S.; Proppe, A. H.; Walters, G.; Nam, D. -H.; Kelley, S.; Hoogland, S.; Voznyy, O.; Sargent, E. H. Acid-Assisted Ligand Exchange Enhances Coupling in Colloidal Quantum Dot Solids. *Nano Lett.* **2018**, 18, 4417-4423.

28. Hong, J.; Hou, B.; Lim, J.; Pak, S.; Kim, B.; Cho, Y.; Lee, J.; Lee, Y.; Giraud, P.; Lee, S.; Park, J. B.; Morris, S. M.; Snaith, H. J.; Sohn, J. I.; Cha, S.; Kim, J. M. Enhanced Charge Carrier Transport Properties in Colloidal Quantum Dot Solar Cells via Organic and Inorganic Hybrid Surface Passivation. *J. Mater. Chem. A* **2016**, 4, 18769-18775.

29. Balazs, D. M.; Dirin, D. N.; Fang, H.; Protesescu, L.; ten Brink, G. H.; Kooi, B. J.; Kovalenko, M. V.; Loi, M. A. Counterion-Mediated Ligand Exchange for PbS Colloidal Quantum Dot Superlattices. *ACS Nano* **2015**, 9, 11951-11959.

30. Ellis, J. L.; Hickstein, D. D.; Schnitzenbaumer, K. J.; Wilker, M. B.; Palm, B. B.; Jimenez, J. L.; Dukovic, G.; Kapteyn, H. C.; Murnane, M. M.; Xiong, W. Solvents Effects on Charge Transfer from Quantum Dots. *J. Am. Chem. Soc.* **2015**, 137, 3759-3762.

31. Sun, J. -K.; Huang, S.; Liu, X. -Z.; Xu, Q.; Zhang, Q. -H.; Jiang, W. -J.; Xue, D. -J.; Xu, J. -C.; Ma, J. -Y.; Ding, J.; Ge, Q. -Q.; Gu, L.; Fang, X. -H.; Zhong, H. -Z.; Hu, J. -S.; Wan, L. -J. Polar Solvent Induced Lattice Distortion of Cubic $CsPbI_3$ Nanocubes and Hierarchical Self-Assembly into Orthorhombic Single-Crystalline Nanowires. *J. Am. Chem. Soc.* **2018**, 140, 11705-11715.

32. Kroupa, D. M.; Anderson, N. C.; Castaneda, C. V.; Nozik, A. J.; Beard, M. C. In Situ Spectroscopic Characterization of a Solution-Phase X-Type Ligand Exchange at Colloidal Lead Sulphide Quantum Dot Surfaces. *Chem. Commun.* **2016**, 52, 13893-13896.

33. Fritzinger, B.; Capek, R. K.; Lambert, K.; Martins, J. C.; Hens, Z. Utilizing Self-Exchange To Address the Binding of Carboxylic Acid Ligands to CdSe Quantum Dots. *J. Am. Chem. Soc.* **2010**, 132, 10195-10201.

34. Santra, P. K.; Palmstrom, A. F.; Tassone, C. J.; Bent, S. F. Molecular Ligands Control Superlattice Structure and Crystallite Orientation in Colloidal Quantum Dot Solids. *Chem. Mater.* **2016**, 28, 7072-7081.

35. Li, M.; Wang, Z.; Zhuo, M.; Hu, Y.; Hu, K.; Ye, Q.; Jain, S. M.; Yang, T.; Gao, X.; Liao, L. Pb–Sn–Cu Ternary Organometallic Halide Perovskite Solar Cells. *Adv. Mater.* **2018**, 30, 1800258.

36. Wang, Z.; Li, M.; Yang, Y.; Hu, Y.; Ma, H.; Gao, X.; Liao, L. High Efficiency Pb–In Binary Metal Perovskite Solar Cells. *Adv. Mater.* **2016**, 28, 6695-6703.

37. Cho, Y.; Hou, B.; Lim, J.; Lee, S.; Pak, S.; Hong, J.; Giraud, P.; Jang, A.; Lee, Y.; Lee, J.; Jang, J. E.; Snaith, H. J.; Morris, S. M.; Sohn, J. I.; Cha, S.; Kim, J. M. Balancing Charge Carrier Transport in a Quantum Dot P–N Junction toward Hysteresis-Free High-Performance Solar Cells. *ACS Energy Lett.* **2018**, 3, 1036-1043.

38. Choi, M. K.; Yang, J.; Kim, D. C.; Dai, Z.; Kim, J.; Seung, H.; Kale, V. S.; Sung, S. J.; Park, C.; Lu, N.; Hyeon, T.; Kim, D. -H. Extremely Vivid, Highly Transparent, and Ultrathin Quantum Dot Light-Emitting Diodes. *Adv. Mater.* **2018**, 30, 1703279.

39. Cao, F.; Zhao, D.; Shen, P.; Wu, J.; Wang, H.; Wu, Q.; Wang, F.; Yang, X. High-Efficiency, Solution-Processed White Quantum Dot Light-Emitting Diodes with Serially Stacked Red/Green/Blue Units. *Adv. Opt. Mater.* **2018**, 6, 1800652.

40. Su, Q.; Sun, Y.; Zhang, H.; Chen, S. Origin of Positive Aging in Quantum-Dot Light-Emitting Diodes. *Adv. Sci.* **2018**, 5, 1800549.

41. Kamminga, M. E.; Fang, H.; Loi, M. A.; ten Brink, G. H.; Blake, G. R.; Palstra, T. T.; ten Elshof, J. E. Micropatterned 2D Hybrid Perovskite Thin Films with Enhanced Photoluminescence Lifetimes. *ACS Appl. Mater. Interfaces* **2018**, 10, 12878-12885.

42. Chiang, C.; Wu, C. A Method for the Preparation of Highly Oriented $MAPbI_3$ Crystallites for High-Efficiency Perovskite Solar Cells to Achieve an 86% Fill Factor. *ACS Nano* **2018**, 12, 10355-10364.

43. Zeng, Q.; Zhang, X.; Feng, X.; Lu, S.; Chen, Z.; Yong, X.; Redfern, S. A. T.; Wei, H.; Wang, H.; Shen, H.; Zhang, W.; Zheng, W.; Zhang, H.; Tse, J. S.; Yang, B. Polymer-Passivated

Inorganic Cesium Lead Mixed-Halide Perovskites for Stable and Efficient Solar Cells with High Open-Circuit Voltage over 1.3 V. *Adv. Mater.* **2018**, 30, 1705393.

44. Zou, Y.; Ban, M.; Cui, W.; Huang, Q.; Wu, C.; Liu, J.; Wu, H.; Song, T.; Sun, B. A General Solvent Selection Strategy for Solution Processed Quantum Dots Targeting High Performance Light-Emitting Diode. *Adv. Funct. Mater.* **2017**, 27, 1603325.

45. Lu, K.; Wang, Y.; Liu, Z.; Han, L.; Shi, G.; Fang, H.; Chen, J.; Ye, X.; Chen, S.; Yang, F.; Shulga, A. G.; Wu, T.; Gu, M.; Zhou, S.; Fan, J.; Loi, M. A.; Ma, W. High-Efficiency PbS Quantum-Dot Solar Cells with Greatly Simplified Fabrication Processing via "Solvent-Curing". *Adv*. *Mater.* **2018**, 30, 1707572.

46. Hassinen, A.; Moreels, I.; De Nolf, K.; Smet, P. F.; Martins, J. C.; Hens, Z. Short-Chain Alcohols Strip X-Type Ligands and Quench the Luminescence of PbSe and CdSe Quantum Dots, Acetonitrile Does Not. *J. Am. Chem. Soc.* **2012**, 134, 20705-20712.

47. Ning, Z.; Voznyy, O.; Pan, J.; Hoogland, S.; Adinolfi, V.; Xu, J.; Li, M.; Kirmani, A. R.; Sun, J.; Minor, J.; Kemp, K. W.; Dong, H.; Rollny, L.; Labelle, A.; Carey, G.; Sutherland, B.; Hill, I.; Amassian, A.; Liu, H.; Tang, J.; Bakr, O. M.; Sargent, E. H. Air-Stable N-Type Colloidal Quantum Dot Solids. *Nat. Mater.* **2014**, 13, 822-828.

48. Kwon, S. M.; Won, J. K.; Jo, J.; Kim, J.; Kim, H.; Kwon, H.; Kim, J.; Ahn, S.; Kim, Y.; Lee, M.; Lee, H.; Marks, T. J.; Kim, M.; Park, S. K. High-Performance and Scalable Metal-Chalcogenide Semiconductors and Devices via Chalco-Gel Routes. *Sci. Adv.* **2018**, 4, eaap9104.

49. Song, J.; Wang, O.; Shen, H.; Lin, Q.; Li, Z.; Wang, L.; Zhang, X.; Li, L. S. Over 30% External Quantum Efficiency Light-Emitting Diodes by Engineering Quantum Dot-Assisted Energy Level Match for Hole Transport Layer. *Adv. Funct. Mater.* **2019**, 29, 1808377.

50. Kim, B. H.; Nam, S.; Oh, N.; Cho, S.; Yu, K. J.; Lee, C. H.; Zhang, J.; Deshpande, K.; Trefonas, P.; Kim, J. Multilayer Transfer Printing for Pixelated, Multicolor Quantum Dot Light-Emitting Diodes. *ACS Nano* **2016**, 10, 4920-4925.

51. Kim, T.; Cho, K.; Lee, E. K.; Lee, S. J.; Chae, J.; Kim, J. W.; Kim, D. H.; Kwon, J.; Amaratunga, G.; Lee, S. Y.; Choi, B. L.; Kuk, Y.; Kim, J. M.; Kim, K. Full-Colour Quantum Dot Displays Fabricated by Transfer Printing. *Nat. Photon.* **2011**, 5, 176-182.

52. Choi, S.; Moon, J.; Cho, H.; Kwon, B.; Cho, N. S.; Lee, H. Partially Pyridine-Functionalized Quantum Dots for Efficient Red, Green, and Blue Light-Emitting Diodes. *J. Mater. Chem. C* **2019**, 7, 3429-3435.

53. Shen, H.; Gao, Q.; Zhang, Y.; Lin, Y.; Lin, Q.; Li, Z.; Chen, L.; Zeng, Z.; Li, X.; Jia, Y.; Wang, S.; Du, Z.; Li, L. S.; Zhang, Z. Visible Quantum Dot Light-Emitting Diodes with Simultaneous High Brightness and Efficiency. *Nat. Photon.* **2019**, 13, 192-197.

54. Lee, K. –H.; Han, C. –Y.; Kang, H. –D.; Ko, H.; Lee, C.; Lee, J.; Myoung, N.; Yim, S. –Y.; Yang, H. Highly Efficient, Color-Reproducible Full-Color Electroluminescent Devices Based on Red/Green/Blue Quantum Dot-Mixed Multilayer. *ACS Nano* **2015**, 9, 10941-10949.

55. Cho, Y.; Lee, S.; Hong, J.; Pak, S.; Hou, B.; Lee, Y. -W.; Jang, J. E.; Im, H.; Sohn, J. I.; Cha, S.; Kim, J. M. Sustainable Hybrid Energy Harvester Based on Air Stable Quantum Dot Solar Cells and Triboelectric Nanogenerator. *J. Mater. Chem. A* **2018**, 6, 12440-12446.

56. Cho, Y.; Giraud, P.; Hou, B.; Lee, Y.; Hong, J.; Lee, S.; Pak, S.; Lee, J.; Jang, J. E.; Morris, S. M.; Sohn, J. I.; Cha, S.; Kim, J. M.; Charge Transport Modulation of a Flexible Quantum Dot Solar Cell Using a Piezoelectric Effect. *Adv. Energy Mater.* **2018**, 8, 1700809.

57. SalmanOgli, A.; Rostami, A. Investigation of Electronic and Optical Properties of (CdSe/ZnS/CdSe/ZnS) Quantum Dot–Quantum Well Heteronanocrystal. *J. Nanoparticle Res.* **2011**, 13, 1197-1205.

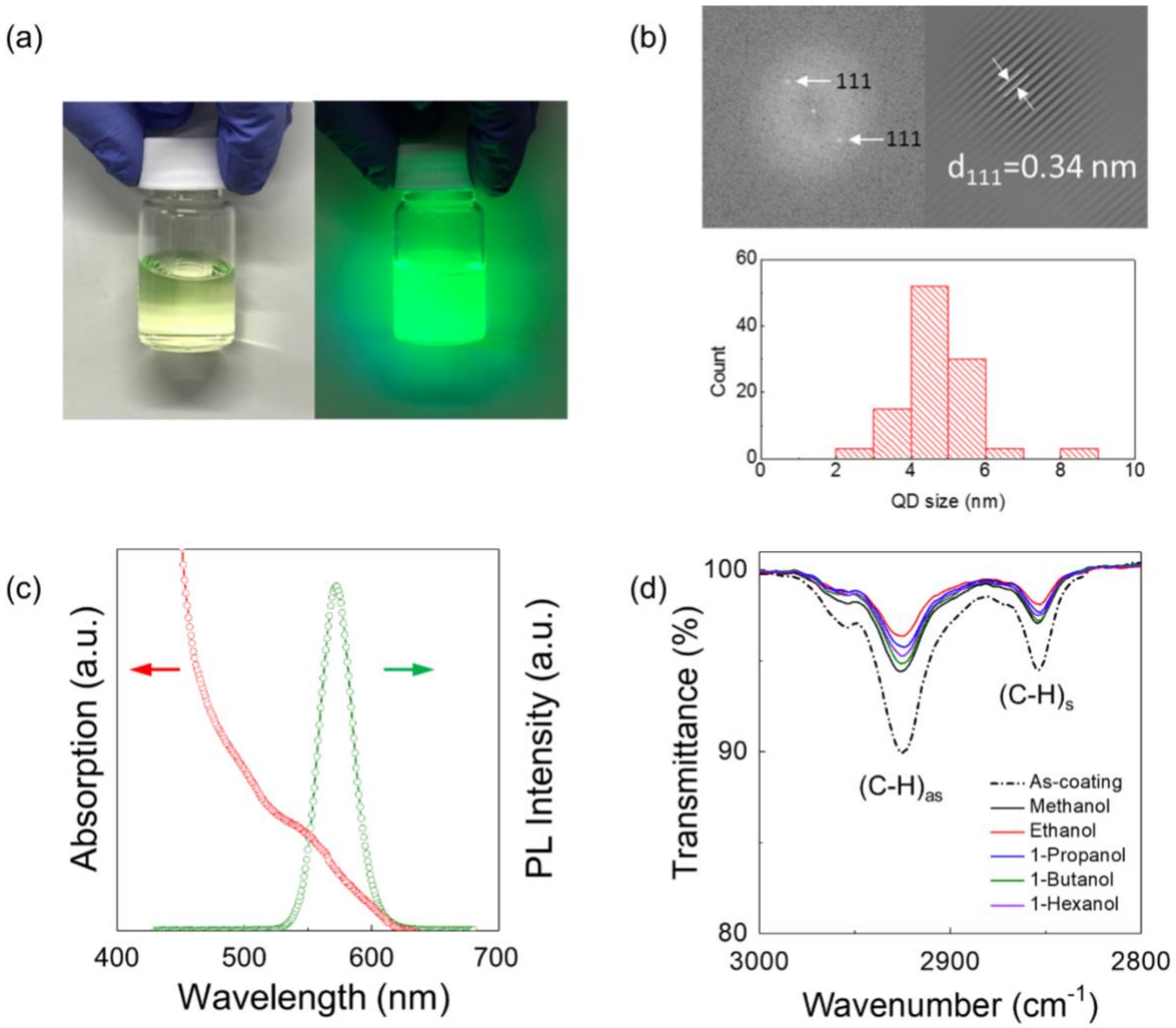

Figure 1. (a) Digital images of CdSe@ZnS QD solution under ambient light (left) and UV light (right). (b) Fast-fourier transformed high resolution TEM diffraction and histogram of QD sizes. (c) Absorption and PL spectra of CdSe@ZnS QDs. (d) FTIR measurement results of a QD film treated by different kinds of protic solvents.

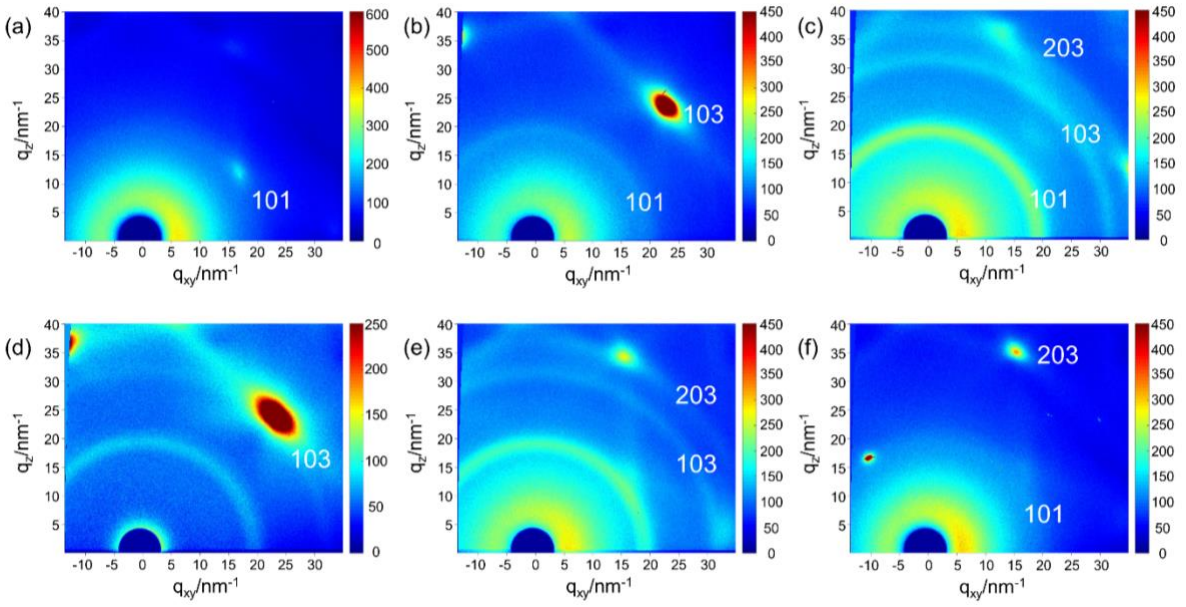

Figure 2. 2D GIXRD patterns of the QD films with: (a) untreated, (b) methanol, (c) ethanol, (d) 1-propanol, (e) 1-butanol and (f) 1-hexanol. The diffraction peaks are highlighted in the 2D GIXRD images.

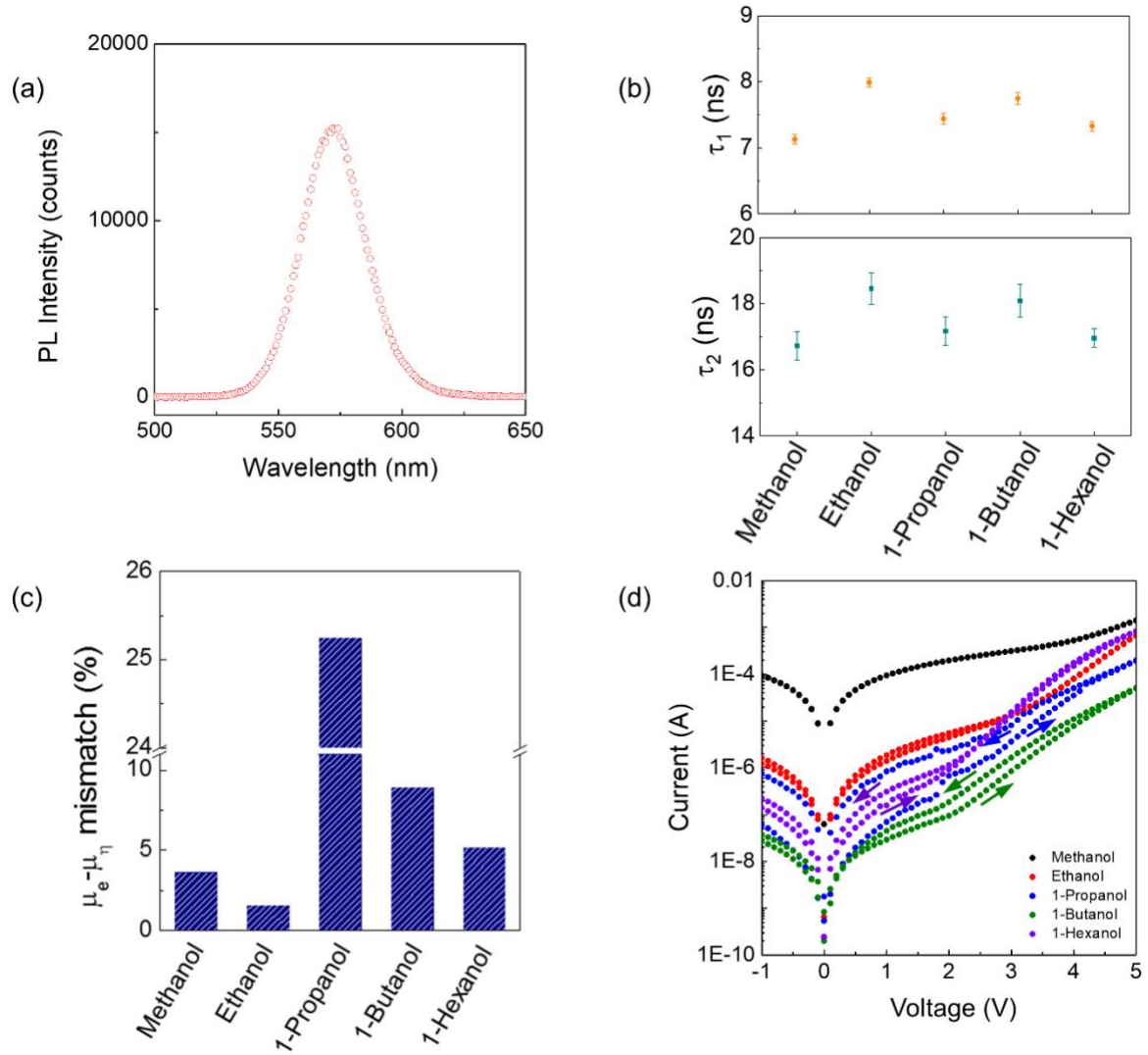

Figure 3. (a) The PL emission spectrum of the QD film treated by ethanol. (b) exciton lifetime of QD films treated by different poly-alkyl alcohol solvents. (c) Calculated electron and hole mobility mismatch in percentage and (d) hysteresis curves of QD-LEDs with respect to different poly-alkyl alcohol solvents.

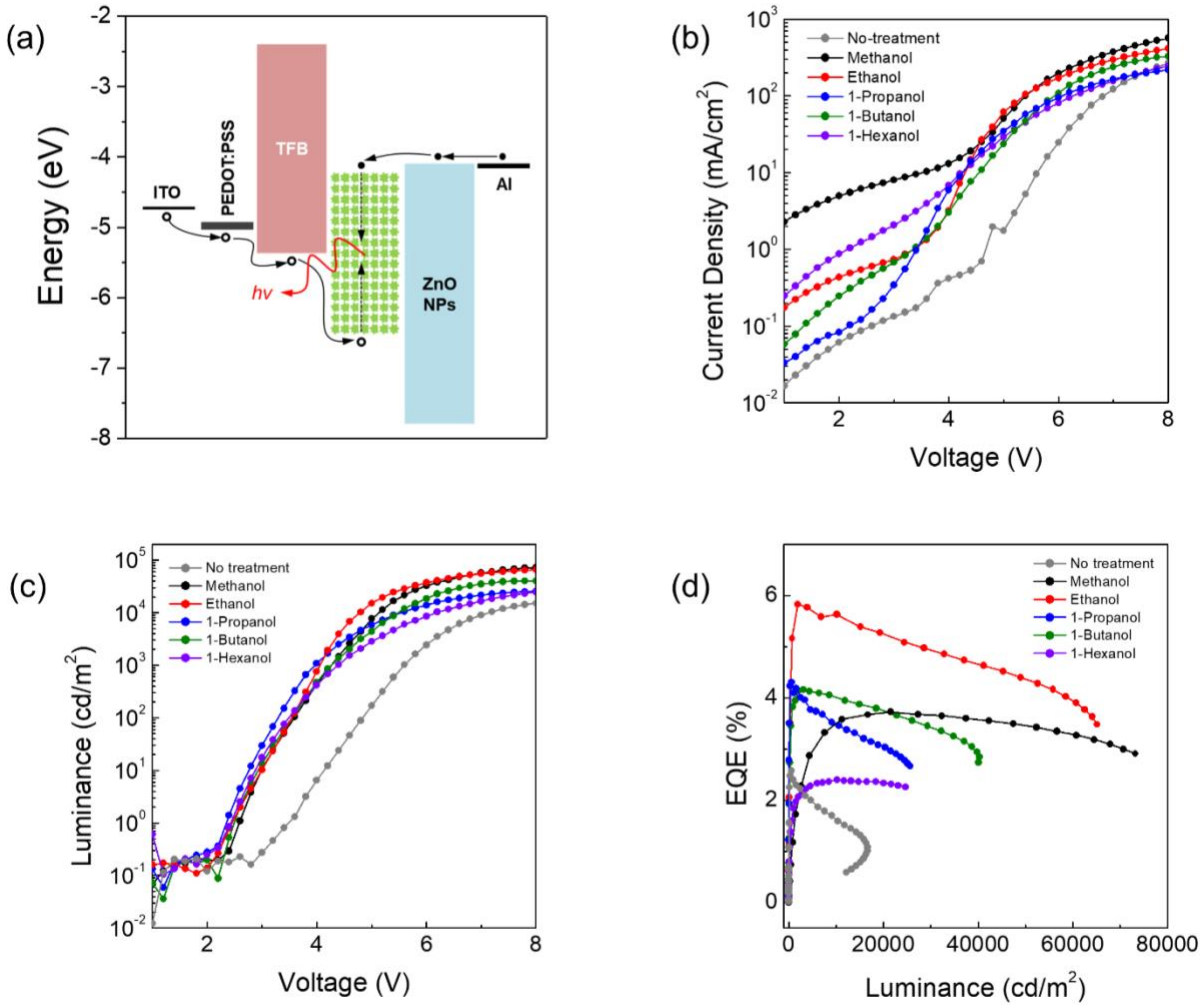

Figure 4. (a) Flat-band energy level diagram. (b) Current density and (c) luminance characteristics for QD-LEDs as a function of voltage applied. (d) EQE of QD-LEDs as a function of luminance.

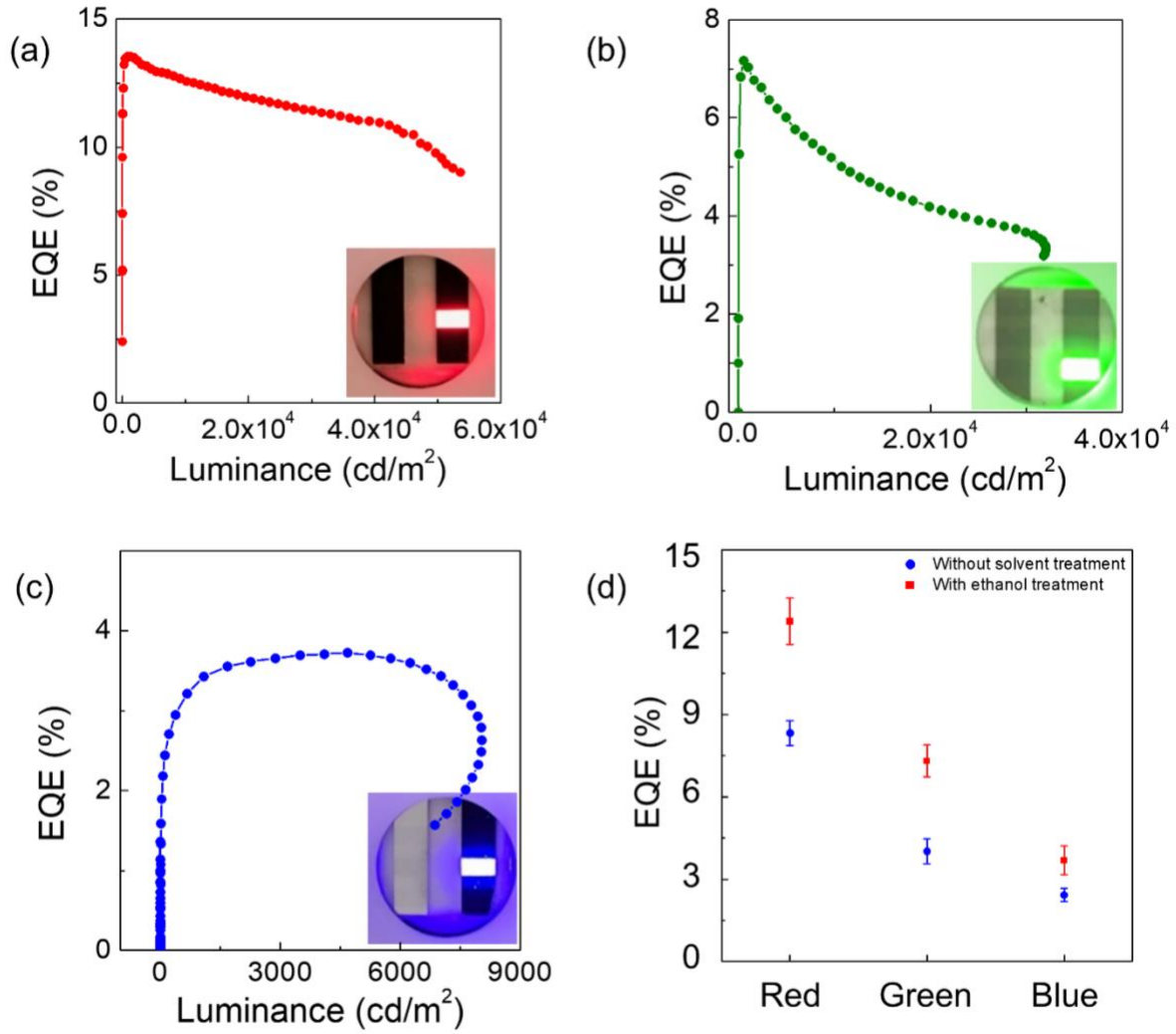

Figure 5. Luminance-EQE characteristic of the (a) Red, (b) Green, and (c) Blue QD-LED. (d) Average EQE values of Red, Green, and Blue QD-LEDs.

Table 1. Electroluminescence performance of QD-LEDs treated by different solvent: L_{max} is maximum luminance; η_A is current efficiency; η_P is power efficiency; η_{EQE} is EQE; and L_{1000} is luminance at 1000 cd m^{-2}.

Green QD-LED	V_{on} (V)	L_{max} (cd m^{-2})	η_A (cd A^{-1})		η_p (lm W^{-1})		η_{EQE} (%)	
			Peak	@L_{1000}	Peak	@L_{1000}	Peak	@L_{1000}
Methanol	2.6	73180	16.85	5.95	9.77	4.38	3.72	1.30
Ethanol	2.4	65120	26.65	24.27	18.20	17.15	5.83	5.30
1-Propanol	2.4	25630	19.25	18.40	16.49	14.66	4.19	4.14
1-Butanol	2.5	40320	18.76	17.45	12.92	12.87	4.15	3.86
1-Hexanol	2.5	24690	10.74	1.84	6.04	5.85	2.39	1.82

Table 2. Electroluminescence performance of Red, Green, and Blue QD-LEDs.

	V_{on} (V)	L_{max} (cd m^{-2})	η_A (cd A^{-1})		η_p (lm W^{-1})		η_{EQE} (%)		
			Peak	@L_{1000}	Peak	@L_{1000}	Peak	@L_{1000}	Avg.
R	1.8	53610	19.29	19.29	26.60	24.24	13.55	13.54	12.40 ± 0.85
G	1.9	32020	30.89	30.43	38.26	34.14	7.17	7.03	7.30 ± 0.59
B	3.1	8037	1.88	1.70	1.03	1.03	3.73	3.43	3.69 ± 0.53

Table of Contents